Control of the Lasing Slice by Transverse Mismatch in an X-Ray Free-Electron Laser

Yu-Chiu Chao, Weilun Qin, Yuantao Ding, Alberto A. Lutman, and Timothy Maxwell

Control of lasing slice by transverse mismatch in an X-ray free-electron laser

Yu-Chiu Chao,[1,*], Weilun Qin[1,2], Yuantao Ding[1], Alberto A. Lutman[1], Timothy Maxwell[1]

[1]*SLAC National Accelerator Laboratory, Menlo Park, CA 94025 USA*
[2]*Institute of Heavy Ion Physics, School of Physics, Peking University, Beijing 100871, China*

We demonstrated selective slice-dependent lasing by controlling the matching to the undulator of different slices within an electron bunch. The slice-dependent mismatch was realized through quadrupole wakefield generated in a corrugated structure. A deterministic procedure based on empirical beam transport and phase space information is used to match selected slices by turns to lase in the undulator while keeping all other slices from lasing, thus staying fresh. Measurements of time-resolved electron bunch energy loss by a transverse deflecting cavity confirmed the predicted behavior.

In an effort to meet increasing demands of the wide scientific community, X-ray free-electron laser (XFEL) pulse customization has been a very active field of investigation. These involve techniques to tailor the temporal X-ray profile such as in double-pulse operations, to control the X-ray's polarization, and to manipulate spectral properties to either narrow photon bandwidth or differentially set photon pulse energies in the so-called multi-color operation. Two-color X-ray pulses for pump-probe experiments have been first demonstrated in a split undulator scheme [1], while independent two-color schemes existed in longer wavelength regimes [2]. Subsequent developments led to wide color separation [3] and high intensity operation [4]. Double X-ray pulses have been used to perform ultrafast studies of X-ray induced phenomena [5,6]. Narrow bandwidth and wavelength stability were achieved with self-seeding schemes [7,8,9] to study the dynamics of warm dense matter systems [10] and for X-ray absorption spectroscopy [11]. Polarization control required by circular dichroism studies [12,13] was made possible by special insertion devices such as the Apple-II type of undulators [14,15,16], or the Delta undulator [17]. Another advance in beam and undulator manipulation involves nonlinear harmonic generation in a helical undulator to produce optical vortices at the second harmonic [18] operating in the extreme UV.

Continuing innovation in slice-dependent lasing control techniques has been instrumental in these advances in FEL experiments [19,20,21]. The work reported in this Letter represents a new approach in this line of developments. One of its implications pertains to the "fresh-slice" technique, first demonstrated in [22] where the temporal slice selected for lasing develops an energy spread in the process, while the rest of the bunch preserves its energy coherence and therefore remains fresh. Unlike other techniques to control lasing slices that irreversibly spoil the electron bunch [19,20,21], in the fresh-slice scheme the lasing-suppressed slices retain full lasing capability in the downstream undulator sections. This enabled multi-color operation combining the high intensity of a twin-bunch scheme with the customizability of a split undulator in terms of delay range, color separation, independent pointing and polarization control. The combination of fresh-slice with self-seeding has led to power increase in the hard X-rays [23] and can lead to terawatt operation with an ad-hoc machine layout [24]. Recently, femtosecond-long and spectrally coherent SASE X-ray pulses were demonstrated in soft X-ray with an order-of-magnitude power increase compared to competing schemes [25], by amplifying an ultra-short pulse produced in a first stage on the bunch tail, followed by preserved fresh-electrons in two additional amplification stages. With more amplification stages, such technique is predicted to achieve powers exceeding a terawatt in few femtoseconds [26].

The above slice-dependent lasing control has been realized via a time-dependent orbit oscillation along the electron bunch impressed by the transverse wakefield when passing off-axis through an aluminum corrugated structure [19], commonly referred to as the "dechirper" as it was designed to control the time-energy profile of the electron bunches [27]. Alternative devices, such as a radio-frequency deflector, or a quadrupole in a dispersive section have been proposed [28] with the latter demonstrated [29]. However, charge losses and radiation issues due to large variation of the slice orbits are main limiting factors to this scheme. For example, the proposed ten-stage terawatt scheme requires a large slice orbit offset of 1.2 mm in the undulator [26]. Potentially, undulator demagnetization issues [30] could prevent operating orbit-based fresh-slice in high-repetition rate machines such as the European XFEL [31] or the LCLS-II (Linac Coherent Light Source) [32].

An alternative method was recently proposed [33] to realize slice-dependent lasing control while preserving energy coherence of non-lasing slices, thus retaining full fresh-slice advantage. Instead of orbit oscillation, this method uses slice-dependent transverse mismatch of the electron bunch to the undulator to realize slice-wise lasing control. Slice-dependent transverse mismatch can be generated by quadrupole wakefield from the corrugated structure with all bunch slices traveling on-axis, space charge induced focusing at low energy [34], or chromaticity acting on energy chirp along the bunch [33]. Slice-dependent lasing activation/suppression is then controlled by external re-matching into the undulator. In-depth simulation study of this scheme has been done [35].

This method presents a new possibility for customized pulse duration control and retains all operation schemes and performance advantages of the fresh-slice scheme, while being less susceptible to tight orbit tolerances of the next generation high-repetition-rate X-ray FEL machines. It also improves the orbit-based fresh-slice by correcting for any undesirable slice-dependent mismatch from the

same quadrupole wakefield. The combined technique is expected to enhance the production of double pulses for X-ray pump, X-ray probe experiments and create more powerful ultra-short pulses required for pushing forward the frontiers of nonlinear science.
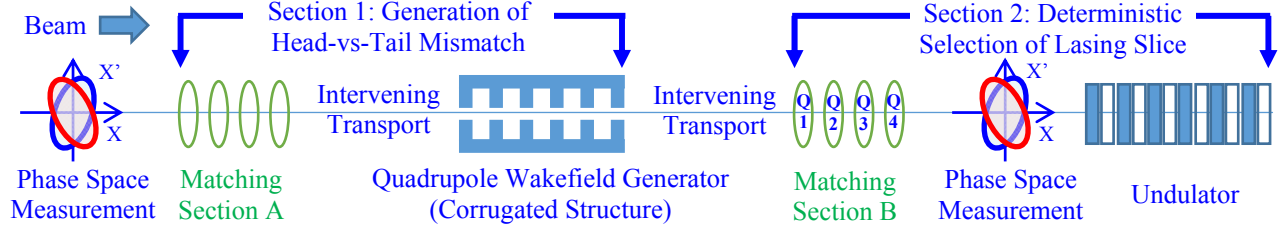
Figure 1. Schematic layout of the LCLS for matching-based slice-dependent lasing control. Section 1 is used to generate and manipulate head-vs-tail mismatch by controlling the transverse beam profile in the corrugated structure (the wakefield generating device). Section 2 is used to deterministically re-match selected temporal slices to the undulator for lasing.

In this Letter we present the first experimental demonstration of matching-based slice-dependent lasing control resulting in fresh-slice operation. The simplest of the mechanisms suggested in [33], namely, quadrupole wakefield from the LCLS corrugated structure [27], is employed to generate time-dependent mismatch. The section of the LCLS machine relevant for the demonstration is schematically represented in Figure 1.

Time-dependent lasing is measured by resolving the changes on the electron bunch time-energy phase space due to lasing process with a downstream X-band Transverse Deflecting Cavity (XTCAV) [36]. A method adopted in routine LCLS operation truncates the current peaks, or "horns", at the bunch head and tail, producing a relatively uniform current profile that enables uniform lasing along the entire bunch [37]. In this way, the time-dependent variation of the beam transverse phase space, represented by the Twiss parameters, is minimized. Subsequently, the empirical electron transport matrices are determined from systematically perturbed electron orbits [38,39], and the electron bunch phase space characteristics, in terms of projected emittance and Twiss parameters, measured at the locations shown in Figure 1.

Section 1 depicted in Figure 1 is used to achieve optimal slice dependent mismatch in the electron bunch, caused by quadrupole wakefield induced on the corrugated structure surfaces. A large head-vs-tail mismatch Φ, defined as [33]

$$\Phi = (1/4)\,\mathrm{Tr}\left(\Sigma_{Head}^{-1} \cdot \Sigma_{Tail}\right),\qquad (1)$$

is desirable, where Σ_{Head} (Σ_{Tail}) is the normalized head (tail) beam covariance matrix

$$\Sigma^{mn} = \frac{1}{N}\sum_{i=1}^{N} X_i^m X_i^n,\ i=1,\cdots N;\ m,n=1,2,3,4 \quad (2)$$

for an ensemble of N particles each having coordinates X^1 to X^4 for the 2 transverse positions and 2 angles. The mismatch factor Φ is a dimensionless measure of degree of phase space mismatch between two beam distributions, in this case the head slice and the tail slice with respective Σ's. Φ equals 1 when head and tail are matched, and increases with growing head-vs-tail mismatch. The head-vs-tail mismatch Φ is frozen once the beam leaves the corrugated structure. In addition, it is desirable to have sufficiently large beam into the corrugated structure to enhance the induced mismatch, while ensuring manageable beam size inside and downstream of the corrugated structure for lossless transport. When needed, Matching Section A can be brought in to achieve optimal trade-off between the above criteria on beam characteristics entering the corrugated structure. A detailed analysis of such trade-off has been presented in [35].

Section 2 depicted in Figure 1 is used to turn on lasing of a specific slice by matching it into the undulator based on optimal matching condition empirically defined at the start of the experiment, while suppressing lasing on all other slices due to the inter-slice mismatch Φ created in Section 1. Matching solutions are calculated based on measured beam phase space, measured machine transfer matrices, and theoretical corrugated structure wakefield model [27], using standard optimization tools or a deterministic matching algorithm [33] for more demanding cases. By dimensionality arguments, 4 quadrupoles are needed for full phase space control on arbitrary input beam. Depending on the input, some quadrupoles may be exerted less than others in a given case.

This scheme has been successfully demonstrated at the LCLS for both hard X-ray (7.7 keV photon energy) and soft X-ray (0.7 keV) FELs. The hard X-ray demonstration is described in detail below covering procedures common to both regimes. Aspects particular to the soft X-ray regime is discussed in addition.

We first needed to confirm that, once the corrugated structure was inserted, the criteria for sufficient head-vs-tail mismatch and contained beam transport would be satisfied. This was verified by applying the wakefield model [27] to the empirically determined electron beam phase space entering the corrugated structure under the condition of full-beam lasing. Table 1 gives these electron beam parameters and Figure 2 shows the calculated head-vs-tail mismatch induced by the corrugated structure. The corrugated structure was then inserted at a gap of 1.0 mm. The structure gap was

accurately adjusted to achieve a negligible residual bunch orbit in the undulator, with all orbit feedbacks disabled, thus avoiding lasing suppression due to orbit oscillation that would otherwise complicate the interpretation of the experiment. Under this condition only the head of the electron bunch, unaffected by the wakefield, was lasing in the undulator. Lasing by the rest of the bunch was suppressed due to large mismatch to the undulator lattice.

The Matching Section B is then used to selectively match different segments of the electron bunch to the undulator. For expediency the bunch is divided into 10 temporal slices, and solutions for all even slices (2, 4, 6, 8, 10) computed and implemented in turn. All slice matching solutions were derived from beam-based measurements and the corrugated structure wakefield model (see Figure 3). This indexing is extended to include "slice 0", denoting the beam and machine state with the corrugated structure inserted, but no re-matching by Matching Section B, thus only the leading edge of the bunch is matched to the undulator.

Figure 4 summarizes the outcome of the above procedure applied to hard X-ray lasing. Figures 4(a-e) correspond to matching of slices 2, 4, 6, 8 and 10. The top part of each graph is the measured longitudinal phase space (energy vs time) of the electron beam streaked by the transverse deflecting cavity (XTCAV) [36]. The bottom part of each graph shows the corresponding reconstructed X-ray pulse temporal profile. The resolution of the measurement is insufficient to resolve single longitudinal SASE (self-amplified spontaneous emission) spikes. The progression of lasing sites closely tracked the intended matched slices, and equivalent photon power generated by lasing slices (20-40 GW peaks) closely matched that of the original optimized full-bunch lasing, indicating efficient lasing from all individually matched slices. The procedure was robust in the sense that one could move between different slice-matching solutions in either direction and obtain reproducible results.

Figure 5 extracts characteristics of each lasing slice (2, 4, 6, 8, 10) out of ensembles of data accumulated under each slice matching condition, in terms of their temporal positions and durations within the bunch. Each ensemble size is on the order of 100. The monotonic migration of temporal position, almost across the entire bunch length, closely matches lasing sites selected by the matching algorithm, while preservation of the wakefield imprint is

clearly visible in the slice duration trend from head to tail, consistent with the parabolic shape of mismatch Φ due to quadrupole wakefield [27] as suggested in Figure 2.
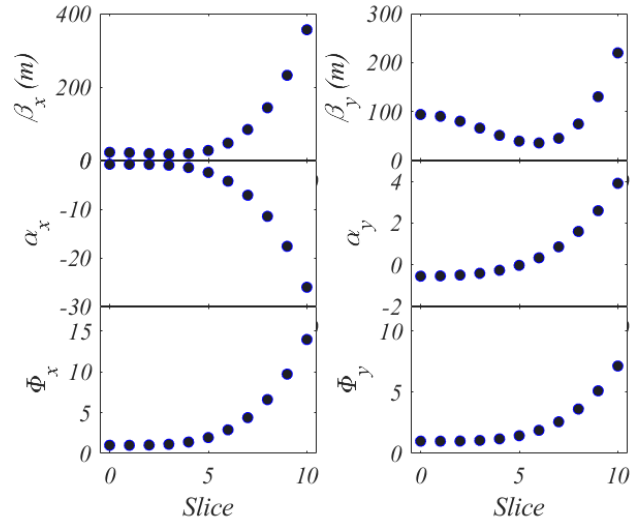
Figure 2. Slice Twiss parameters β (in meter) and α, and mismatch factors Φ, in X and Y planes at the entrance to the undulator as functions of slice index inside the bunch. Mismatch factors are computed relative to bunch head (position 0), based on beam based measurements and corrugated structure quadrupole wakefield model.
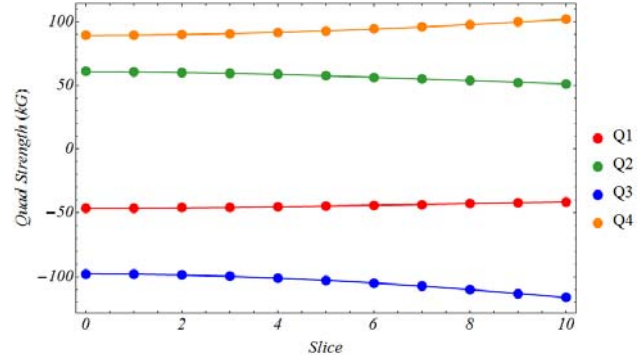
Figure 3. Evolution of the 4 quadrupole strengths (Q1-4 in Figure 1) in Matching Section B to actuate undulator matching of slices 1 through 10 (dots) along the bunch for the hard X-ray experiment. Slice position 0 corresponds to initial quadrupole configuration.

Figure 4. Measured longitudinal phase space of the electron bunch in the hard X-ray experiment, under matching conditions for slices 2, 4, 6, 8, 10 (left to right). In each graph the top portion shows the beam distribution in the space

of energy (MeV) vs time (fs) around beam centroid. The bottom portion reconstructs the X-ray power temporal profile obtained by comparing the time-resolved electron bunch lasing footprint against commensurate bunch with lasing process   suppressed.   The   same   scheme   is   used   in   Figure   6.

The same procedure was also applied in the soft X-ray regime. Electron bunch compression was relaxed (see Table 1) to enhance the head-to-tail mismatch in order to achieve cleaner demarcation between the lasing and suppressed slices. The outcome of this experiment is shown in Figure 6. While the lasing slices were not as sharply defined, determinism and predictive power of the method was unmistakable. Possibility of further manipulating electron beam phase space into the corrugated structure with Matching Section A to enhance the lasing slice definition is being considered.

In this Letter we demonstrated for the first time the technique of slice-dependent control based on transverse matching, and the resulting fresh-slice operation. Besides being a new FEL slice manipulation and pulse customization technique, it retains the benefits of fresh-slice operation without requiring a large electron bunch orbit in the undulator. Therefore it is well-adapted to higher repetition rates and tighter beam loss tolerances typical of superconducting radio-frequency (SRF) machines compared to its orbit-based counterpart. This class of machines will include the European XFEL [31], the LCLS-II [32], and the Shanghai Coherent Light Facility (SCLF) [40]. The scheme can also enhance the orbit-based fresh-slice by deterministically re-matching the slices to the undulator, and by optimizing corrugated structure focusing effect on the slices through Matching Section A in Figure 1. The method as demonstrated allows deterministic control of pulse duration as a function of selected lasing slice due to the nonlinear nature of the wakefield. Shorter lasing slices are achievable with smaller gap settings of the wakefield device or by increasing the transverse size of the beam at the device location. More systematic simulation and experimental studies are needed to probe the limit of achievable pulse duration, as other factors besides the time-dependent mismatch influence the achieved X-ray duration (e.g. post saturation undulator taper). The experimental observation so far suggests that, for typical LCLS hard X-ray parameters, a sub-10 femtosecond pulse duration should be routinely achievable. Among X-ray FEL enabled sciences that can benefit from such schemes, we cite non-linear science experiments in attaining higher power and shorter pulses available with multi-stage amplification, and X-ray pump, X-ray probe experiments in attaining higher X-ray power (an order of magnitude larger than the regular split undulator) and acquiring the ability of scanning temporal delay in the very first few femtoseconds, otherwise prevented due to the intrinsic delay [1,3]. Experiments using seeding based FEL can also benefit from increased power in such schemes.
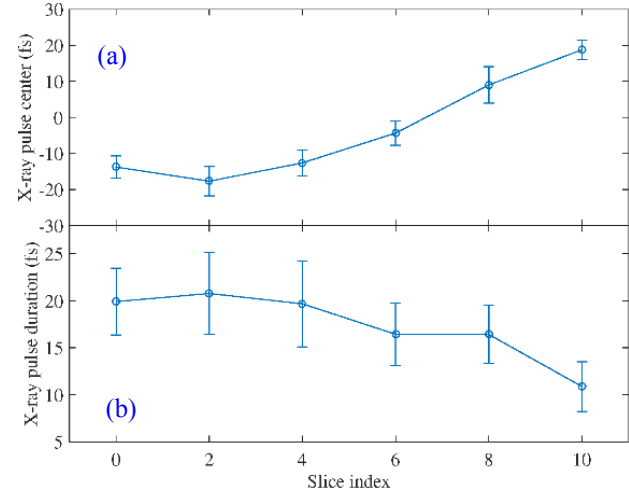
Figure 5. Centroid locations relative to bunch center (a), and durations (b), both in fs, of lasing slices 2, 4, 6, 8, 10 from the hard X-ray experiment. Each data point is averaged over an ensemble of analyzed XTCAV images of nearly equal bunch length, with standard deviation indicated by the error bar. The ensemble size is on the order of 100. Deviation from monotony at position 0, not part of the re-matching procedure, is due to artefact from an overall offset between theoretical and empirical transport models.
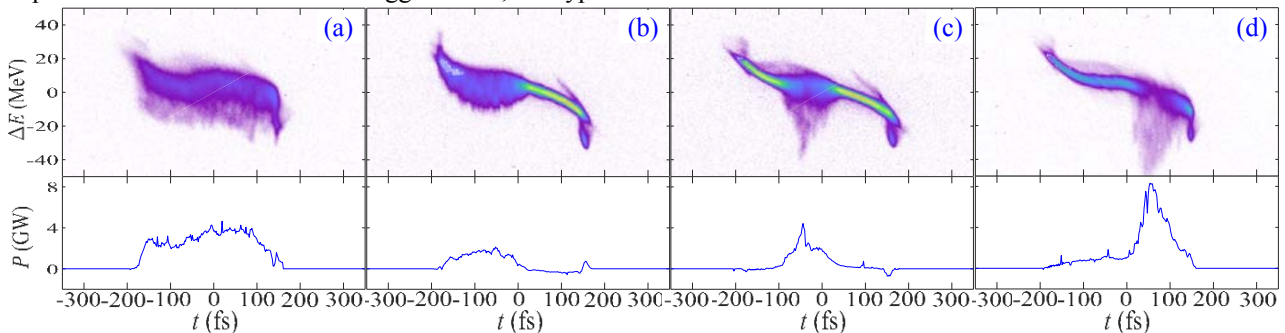
Figure 6. Measured longitudinal phase space of the electron bunch in the soft X-ray experiment. (a): Entire bunch matched to undulator (no head-vs-tail mismatch); (b-d): Only selected slice 0, 5 and 10 matched to undulator. In each graph the top portion shows the beam distribution in the space of energy (MeV) vs time (fs) around beam centroid. The bottom portion shows the reconstructed X-ray power temporal profile (GW) as function of location in the bunch (fs).

Parameter	Hard X-ray	Soft X-ray	Unit
Electron Energy	12.97	3.890	GeV
Bunch charge	177	180	pC
Bunch length	50	216	fs
Peak Current	3800	800	A
Norm. Emittance X/Y	1.18/1.18	1.16/0.880	μm
Structure full gap	1.00	1.53	mm
β_X/β_Y into structure	73.6/58.6	5.30/80.4	m
α_X/α_Y into structure	1.48/4.89	-0.87/10.15	
$\Phi_{X/Y}$	14.0/7.14	1.5/38.0	
Photon energy	7.7	0.7	keV

Table 1. Beam and machine parameters of matching-based fresh-slice experiments at the LCLS.

*ychao@slac.stanford.edu

References

[1] A. Lutman, et al, Phys. Rev. Lett. 110, 134801 (2013).
[2] G. De Ninno et al. Phys. Rev. Lett. 110, 064801 (2013)
[3] T. Hara et al., Nature Communications 4, 2919 (2013)
[4] A. Marinelli et al., Nature Communications 6, 6369 (2015).
[5] K.R. Ferguson et al. Science Adv. 2 e1500837 (2016)
[6] A. Picon et al., Nature Communications 7, 11652 (2016)
[7] J. Amann et al. Nat Photon 6, 693 (2012).
[8] A. Lutman, et al, Phys. Rev. Lett. 113, 254801 (2014).
[9] D. Ratner, et al, Phys. Rev. Lett. 114, 054801 (2015).
[10] L.B. Fletcher et al. Nature Photonics 9, 274-279 (2015).
[11] T. Kroell et al. Optics Express 24, 22469.
[12] D. Higley et al. Rev. Sci Instrum. 87, 033110 (2016)
[13] G. Hartmann et al. Rev. Sci. Instrum. 87, 083116 (2016)
[14] E. Allaria et al., Nat. Photon. 7, 913 (2013).
[15] E. Allaria et al., Nature Communications 4 (2013), 10.1038/ncomms3476
[16] E. Allaria et al. Phys. Rev. X 4, 041040 (2014)
[17] A. Lutman et al. Nat Photon. 10, (2016). 468-472 (2016)
[18]. P. Rebernik Ribič et al., Phys. Rev. X 7, 031036 (2017)
[19] P. Emma, et al. Phys. Rev. Lett. 92, 074801 (2004).
[20] Y. Ding, et al. Applied Physics Letters 107, 191104 (2015),
[21] A. Marinelli, et al, Phys. Rev. Lett. 116, 254801 (2016).
[22] A. Lutman et al. Nat Photon. 10, (2016). 745–750 (2016)
[23] C. Emma et al. Applied Physics Letters 110, 154101 (2017)
[24] C. Emma, K. Fang, J. Wu, and C. Pellegrini, Phys. Rev. Accel. Beams 19, 020705 (2016).
[25] A. A. Lutman, M. W. Guetg, T. J. Maxwell, J. P. MacArthur, Y. Ding, C. Emma, J. Krzywinski, A. Marinelli, and Z. Huang, Phys. Rev. Lett. 120, 264801.
[26] E. Prat, F. Löhl, and S. Reiche, Phys. Rev. ST Accel. Beams 18, 100701 (2015).
[27] K. Bane, G. Stupakov, and I. Zagorodnov, Phys. Rev. Accel. Beams 19, 084401 (2016).
[28] E. Prat, S. Bettoni, and S. Reiche, Nucl. Instrum. Methods Phys. Res. A 865, 1 (2017).
[29] M. W. Guetg, A. A. Lutman, Y. Ding, T. J. Maxwell, and Z. Huang, Phys. Rev. Lett. 120, 264802.
[30] M. W. Guetg, P. J. Emma, M. S. Leitner, J. Welch, and F. Zhou. Collimation system design for LCLS-II, Proceedings of 7th International Particle Accelerator Conference, Busan, Korea, 2016.
[31] H. Weise, Proceedings of LINAC2016, East Lansing, Michigan, USA, pp 7-11 (2016).
[32] J. N. Galayda, Proceedings of LINAC2014, Geneva, Switzerland, pp 404-408 (2014).
[33] Y.-C. Chao, SLAC-PUB-16935 (2016); arXiv:1704.08813.
[34] B. E. Carlsten, Nucl. Instrum. Methods Phys. Res. A 285, 313 (1989).
[35] W. Qin, Y. Ding, A. A. Lutman, and Y.-C. Chao, Phys. Rev. Accel. Beams 20, 090701 (2017).
[36] C. Behrens et al., Nat. Commun. 5, 3762 (2014).
[37] Y. Ding et al., Phys. Rev. Accel. Beams 19, 100703 (2016)
[38] Y.-C. Chao, Proceedings PAC07, p780.
[39] P. Emma and W. Spence, Proceedings PAC91, p1549.
[40] Z. T. Zhao et al, presentation MOP055, Proceedings of FEL Conference 2017, to be published.